Effect of Viscous and Thermal Forcings on Dynamical Features of Swimming of Microorganisms in Nanofluids

S. Sharafatmandjoor[*,1,2]*, and C. S. Nor Azwadi*[3]

[1]Department of Mechanical and Aerospace Engineering, Science and Research Branch, Islamic Azad University, Tehran, Iran.
[2]George Brown College, Canada.
[3]Faculty of Mechanical Engineering, University of Technology Malaysia, 81310 Skudai, Johor, Malaysia.
[*]*sharafatmand@srbiau.ac.ir*

Abstract – *As a practical dynamical system approach to analyse microorganisms, we have used the system identification approach to develop a framework that is capable of introducing external forcing on a time series data. For this goal, a two-equation deferential equation system for time evolution of the experimental parallel velocity values of head of a bull spermatozoon during circular swimming [1] is reconstructed. The planar movement of the sperm is shown to be modelled well with this deferential system for three different cases. We also present a least-squares analysis on a system with more sampled data with fewer points used in the time marching of the deferential system and show how the system can represent the real pattern approximately. Following this idea we bring a linearized model of the system and investigate it near its equilibrium points on a Trace-Determinant chart. Finally, we show how this straightforward system can be employed where external viscous and/or thermal forcings due to swimming in a nanofluid is a dominant phenomenon. We bring a phase portrait demonstration of the time evolution of the system to highlight the main modifications in the dynamics.* ***Copyright © 2016 Penerbit Akademia Baru - All rights reserved.***

Keywords: System-Identification, Microorganism, Nanofluid, Trace-Determinant Chart, Dynamical System

1.0 INTRODUCTION

Among many other applications experimental data represent the mathematical structure of the underlying systems. Traditionally, differential equations have been employed to model the physical assumptions adopted for real world problems. Conversely, in the so-called system identification approach governing equations of the systems are reconstructed by proper selection of a mathematical form from the experimental time series. One of the challenges in these methods is treating high-dimensional disturbances in nonlinear systems where overfitting the data is often inevitable [2]. The other important concerns are selecting a proper function space and considering the existing physical interactions of the dependent variables [3]. With a careful selection of the parameters, the resulted equations are needed to contain sufficient dynamical information about the system [3]. Theoretically, for systems with adequate low-dimensional components, even when the system is of a high dimension or it is polluted by

noise, the system identification algorithm can still represent some useful means of approximation [2]. In practice, adopting a parsimonious form of the model usually prevents the excitation of unphysical dynamical regimes.

System identification methods have been used in many branches of science and engineering via modern non-linear analysis. The first attempts were mainly focused on seeking the local dynamics by capturing the short-range behaviours in the related attractor that are classified as flow method [5]. Later, the long-term effects proposed by [5] was employed together with the concept of the flow method to form the talented trajectory method [2]. Alternatively, a chaotic time series can be synchronized with a known structured differential system by obtaining the unknown parameters of the model. The synchronization algorithms can be applied via *e.g.* multiple shooting methods which are usually coupled with a high-dimensional minimization problem [6]. For a complete review on the issue one can refer to [2].

In this work, we have applied the system identification idea to the experimental time series of an experiment on the bull sperm swimming. Our motivation was the fact that viscous effects are the essential factor in migration of a successful sperm through the female tract. The complex physics of highly viscous invaginated media restricts the number of sperms ever succeed to only tens. This fact urges researchers to study the ways that they can guide a sperm to increase the chance of fertilization [7]. In other words, a simple non-dimensional analysis shows that the creeping flow around a sperm and other microorganisms is dominated by viscous effects and the governing equations of motion reduce to a balance between pressure gradients and viscous terms. Therefore, any change in the value of viscosity affects the motion drastically. Presenting an ordinary differential equation (ODE) model for the problem of sperm movement is important because we can make a basis for more complex systems with added spatial degrees of freedom by assessing the change in viscosity of the surrounding flow. After proposing the ODE, the next part of the paper is devoted to study the effect of changing the parameters of the linearized equation near the equilibrium points.

In the last part we have investigated the effect of adding nanoparticles to the pure media. This technique is employed mostly to study the enhancement in thermal conductivity of nanofluids [8-14]. On the other hand, the change in the viscosity of the suspension can be modeled via an experimental relation as a single-phase system [15]. Since the nanoparticles are very tiny and the volume fractions are in low range, the suspension has no erosion, sedimentation, pressure change or non-Newtonian side effects [16]. For some relevant applications of the idea see [17-20]. The effect of this external viscous forcing is introduced to the system by forcing the differential system with a proper forcing term borrowed from resistive force theorem (RFT). This theory states that by multiplying the local velocity components by resistance constants it is possible to approximate the force generated by each element. Forcing the dynamical systems with physical external excitations has been proposed and verified by [3].

2.0 MATHEMATICAL MODELING

In this section we present the details of obtaining a proper two-equation system that is tuned to mimic the instantaneous velocity components of head of a bull sperm. The instantaneous velocities measured in a plane that are extracted from [1] are induced by the flagellar beat through circulating swimming in pure water. However the regime of the flow field is assumed to be the creeping flow, the dynamics of the system is basically nonlinear [1]. Therefore, we need to treat the nonlinearities properly.

Here, inspired by [2] we propose a polynomial-based coupled model with ten coefficients designed to get minimized cost functions associated with the error of the model [3].

$$\frac{\delta y}{\delta t} = v \tag{1a}$$

$$\frac{\delta v}{\delta t} = c_1 + c_2 y + c_3 v + c_4 y^2 + c_5 yv + c_6 v^2 + c_7 y^3 + c_8 y^2 v + c_9 yv^2 + c_{10} v^3 \tag{1b}$$

Where the displacement and velocity values are associated with y and v values respectively and the constants $C_1{:}C_{10}$ are to be determined. The structure of the system has been proved to be sufficient to represent the essential nonlinearities of the original data [21]. This format would be desirable when we force the system by adding some acceleration-type forcing terms to the right hand side of the second equation in the last section of the paper.

Our first three test cases are designed and classified based on the length of time samplings. In cases 1, 2 and 3 $\delta t = 9.7E$ - 4, $1.6E$ - 3, and $3.1E$ - 3 respectively. Thus, cases 1 and 3 correspond to the _nest and coarsest time samplings respectively. All these three cases use 10 sampled points. Test case 4 is examined via our least-squares analysis. Its time sampling is analogous to case 3 but it is sampled with 20 points. For cases 1, 2, and 3, the algebraic system is composed by writing equations $1a$ and $1b$ for each point as:

$$\begin{bmatrix} 1 & y_{(1)} & \cdots & v_{(1)}^3 \\ 1 & y_{(2)} & \cdots & v_{(2)}^3 \\ \vdots & \vdots & \ddots & \vdots \\ 1 & y_{(10)} & \cdots & v_{(10)}^3 \end{bmatrix} \times \begin{bmatrix} c_1 \\ c_2 \\ \vdots \\ c_{10} \end{bmatrix} = \begin{bmatrix} \left.\frac{dv}{dt}\right|_{(1)} \\ \left.\frac{dv}{dt}\right|_{(2)} \\ \vdots \\ \left.\frac{dv}{dt}\right|_{(10)} \end{bmatrix} \tag{2}$$

Hereafter, the coefficient matrix, unknown vector and the known vector are denoted by $A_{10\times10}$, $C_{10\times1}$ and $B_{10\times1}$ respectively. In system 2 the subscripts (i), $i \in 1{:}10$ means the corresponding values at points 1 to 10. The approximated displacement y is obtained from the given velocity values using the trapezoidal rule and the differentiations in vector B is computed via second-order differencing directly from the time series. We then apply the standard LU decomposition routine to find the ten unknowns. Table 1 brings the components of vector C for cases 1, 2 and 3. The nonlinearity of the systems makes remarkable discrepancy in the values of the sets.

Having the differential system we then solve the initial value problem with the fourth-order Runge-Kutta method by simply selecting the arbitrary y_0 and experimental v_0. In this study the Runge-Kutta time step is 10 times smaller than the original sampling time step. Left panel of Fig. 1 shows how the reconstructed ODE is consistent with the experimental values for the finest time sampling *i.e.* case 1.

Table 1: Components of the Vector C for cases 1, 2, and 3.

	Case 1	Case 2	Case 3
c_1	7.2E6	-8316.7	-1E5
c_2	3.6E5	1.4E5	-61247.9
c_3	-1.7E5	819.8	4913.6
c_4	2.1E5	6487.5	25179.8
c_5	-26998.2	-796.9	232.4
c_6	1434.7	-3.7	-41.4
c_7	2.6E5	-35003.1	-1050.8
c_8	26745.7	-258.4	-223.1
c_9	216.3	0.9	1.0
c_{10}	-3.9	0.0	0.1

The ODE can also be used for the extrapolation purpose in the short time ranges. If we extract data points with larger sampling time steps, the quality of the prediction of the ODE is reduced. See the middle and right panel of Fig. 1 for the effect of rather large time samplings. However, the ODE estimations are poorer for larger time samplings, the main trend of the data is still captured. Since in our method sets of 10 points are employed for obtaining the values of C, one can apply the following algorithm for different sections of the experimental data and match the boundary values and slopes.
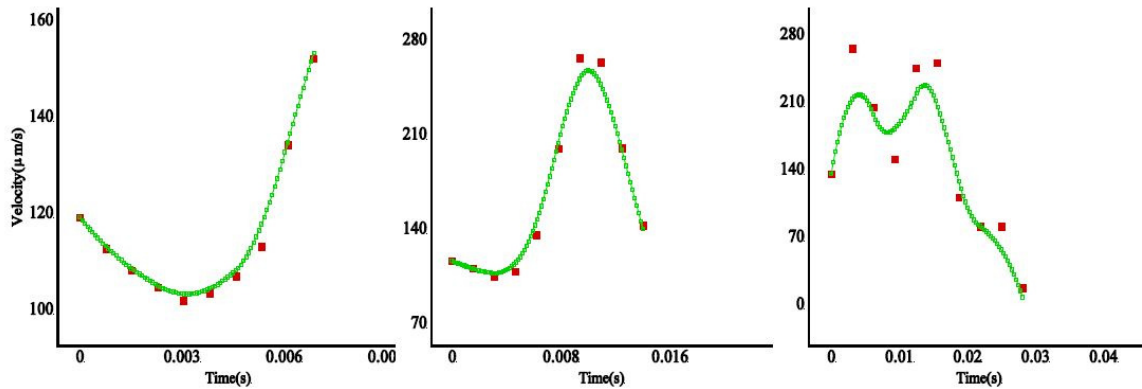
Figure 1: Extracted Experimental Velocity Time Series (red) and the Modeled Values Obtained by Solving the System 1a, and 1b (green). Left, middle and right panels correspond to cases 1, 2 and 3 respectively.

If we wish to use more than 10 data points with one single set of C_1 to C_{10}, least-squares concept would be a wise choice to approximate the over-determined problem [4]. For a n-data point system ($n \rangle 10$) we can pre-multiply either sides of Eqn. 2 by the transpose of the coefficient matrix namely A^T to get:

$$A^T_{10 \times n} A_{n \times 10} C_{n \times 1} = A^T_{10 \times n} B_{n \times 1} \tag{3}$$

The above system leads to a new 10 equation and 10 unknown system and can be solved similar to system 2.

The relative error with respect to the experimental velocity values $u_{(i)}^{ex}$ is defined as:

$$E = \sum_{(i)} \frac{\left| u_{(i)} - u_{(i)}^{ex} \right|}{\left| u_{(i)}^{ex} \right|} \times 100\% \qquad (4)$$

Figure 2 shows the time convergence quality for different samplings. The depicted results compare relative error values E for cases 1, 2 and 3. We can deduce that if we decrease the time step of sampling, the relative errors decay at least with order -2.6. This feature of the results guarantee the time convergence of the method. Conversely, we have found that however decreasing the Runge-Kutta time step tends to better match in each individual time samplings, the gain saturates for very fine Runge-Kutta time steps. This indicates that the sampling enjoys the main contribution in approaching the predicted values to the experiment, while for each sampling time step Runge-kutta time step less than ten times smaller than the sampling time step would not make more gain. Therefore, in this study this ratio has been adopted through all results.
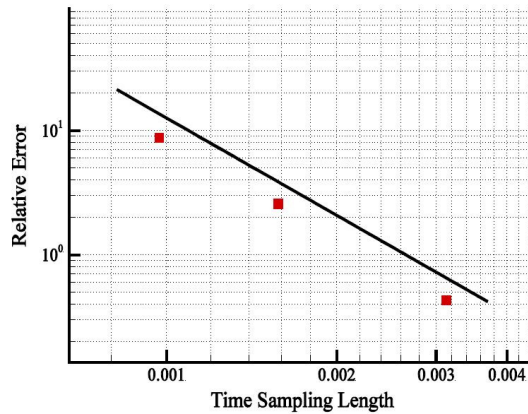
Figure 2: The Relative Error versus Different Sampling Times. Cases 1, 2 and 3 correspond to δt=9.7E-4, 1.6E-3, and 3.1E-3 respectively. Slope of the Solid line is -2.6.

For case 4, Fig. 3 shows the effect of applying the least-squares technique where the original data points are $n = 20$. For this approximation relative error value in equation 4 is 12.96 which is obviously larger than the typical values obtained for the non-least-squares cases. However, the least-squares technique provides the least possible discrepancy between the predictions and the experimental data. Furthermore, we should be aware of the effect of the round-off errors in the computations of the least-squares technique. For example, if we apply the least-squares technique trivially for the 10 points system the components of vector C slightly vary up to second floating point values. Some other methods like singular value decomposition can also be used to solve the over-determined system.

3.0 ANALYSIS OF THE LINEARIZED MODEL

As mentioned before, if a model reconstructs the original experimental data, then its mathematical specifications will give information about the original dynamical features. Therefore, in order to analyze basic dynamics of a system we follow the process of linearization

[22] to have the benefits of the excellent linearity principles theoretical background. This is one of the reasons that researchers seek models that are as simple as possible.
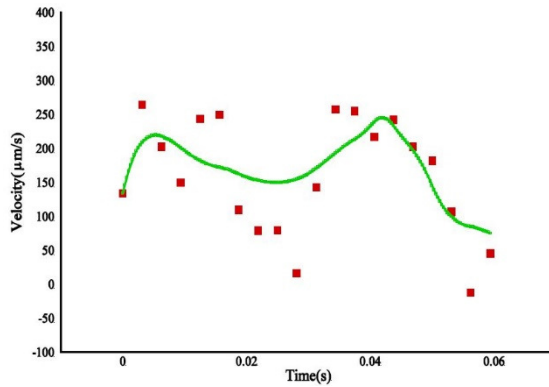
Figure 3: Extracted Experimental Velocity Time Series (red) and the Modeled Values Obtained from Least-squares Technique (green) Corresponding to case 4.

Non-linear systems behave close to their corresponding linear model in the vicinity of the equilibrium points. Thus, we take advantage of modeling the system with the very simple linearized model. The non-homogeneous linearized form of the system 1a and 1b reduces to:

$$\frac{d^2 y}{dt^2} - c_3 \frac{dy}{dt} - c_2 y = c_1 \tag{5}$$

The solution for this model is a superposition of the homogeneous solution and one particular solution for the non-homogeneous equation that is a direct function of $c1$. Here, we investigate the homogeneous part, considering that the trace and determinant of the corresponding system are $c3$ and $-c2$ respectively. Real and complex eigenvalues of the system are seen to be a direct function of these two parameters. Therefore, a low-dimensional assessment of the system is possible. Fig. 4 reveals the corresponding schematic Trace-determinant diagram. In this figure different scenarios of the stability of the manifolds based on different values of the equation parameters are represented schematically.
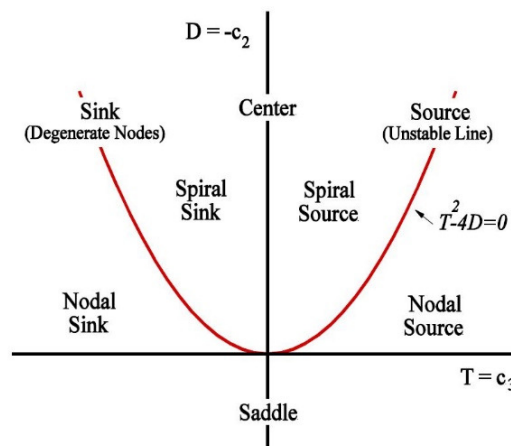
Figure 4: Schematic Trace-Determinant Diagram for Classification of Fixed Points of the Linearized System 5. *Trace = c3, Determinant = -c2.*

4.0 EXTERNAL VISCOUS AND THERMAL FORCING

In order to investigate the effect of extra viscous forcing due to additive nanoparticles we use RFT to explain the force on the sperm. RFT is itself a low-dimensional simplification to the slender body theory where slender filaments are approximated in the zero-Reynolds number limit. RFT is first presented by [23] and its relations are well described in [24] for a helical pattern that is the common movement path for a typical sperm. In RFT the sperm movement is considered as elements travelling with velocity $u = u_\parallel \hat{\eta} + u_\perp \hat{\zeta}$ where $u_\parallel$ and $u_\perp$ are respectively velocities parallel and normal to the tangential vector with unit vectors $\hat{\eta}$, and $\hat{\zeta}$. In addition, the local drag coefficients $c_\parallel$ and $c_\perp$ are assigned to relate the local viscous forces per unit mass to the local velocity components. Here, we deal with the parallel velocity values, since parallel drag force acts corresponds to this velocity component, in a way that the total acceleration tangent to the movement direction can be written as $a_\parallel = -c_\parallel u_\parallel \hat{\eta}$. For a filament moving in a plane through a liquid with viscosity μ far from a solid body RFT approximates the $c_\parallel$ as:

$$c_\parallel = \frac{2\pi\mu}{\ln\left(\dfrac{2\lambda}{r}\right) - \dfrac{1}{2}} \tag{6}$$

In which, λ is the wavelength of the flagellar bending waves, and r is the approximate radius of the filament. For water at 36°C, $\lambda = 66 \pm 8 \mu m$. The length of head of sperm is also about 10 μm. Since, in our creeping flow regime in the lack of inertia the only governing force of the system is the viscous forcing, we introduce the remarkable extra viscous effects due to the added nanoparticles as an additive acceleration term to the second equation of system *1a* and *1b*.

The contribution of adding nanoparticles to change in the viscosity of the base flow (here water) is investigated via experimental relation of Brinkman [15]. In this relation the viscosity of the nanofluid is approximated as a function of the viscosity of the base flow μ_{bf} containing a dilute suspension of nanoparticles with volume fraction ϕ. The formula is valid only for spherical nanoparticles [15]. Based on this relation we can find $\delta\mu$ the change in the viscosity of the medium which is the cause of the extra viscous forcing.

$$\delta\mu = \mu_{bf}\left(1 - \frac{1}{(1-\phi)^{2.5}}\right) \tag{7}$$

For water at $36^o C$, $\mu_{bf} = 0.7 mPas$. This way we can model the nanofluid as a single-phase and approximate the extra acceleration force imposed on the system by using $\delta\mu$ instead of μ in Eqn. 6.

For the effect of temperature change on the viscosity of the surrounding flow we employ the extrapolated values from the experiment of [25]. Fig. 5 shows the solution space of the system corresponding to case 1, 2, and 3 for two typical values ϕ = 0.1 and 0.2 with and without temperature forcings. In this figure the vertical axis is the percentage of deviation of the acceleration and the horizontal axis represents its base velocity values. Based on the figure the acceleration is triggered mostly for some unique velocity values. In fact as the time sampling

is increased from case 1 to case 3 the number of triggered velocity values are increased. Furthermore, for each case we can see that extra volume fractions makes more deviations but with the same trend. On the other hand increasing the temperature from 36 to 38°C moderates this implied deviation.
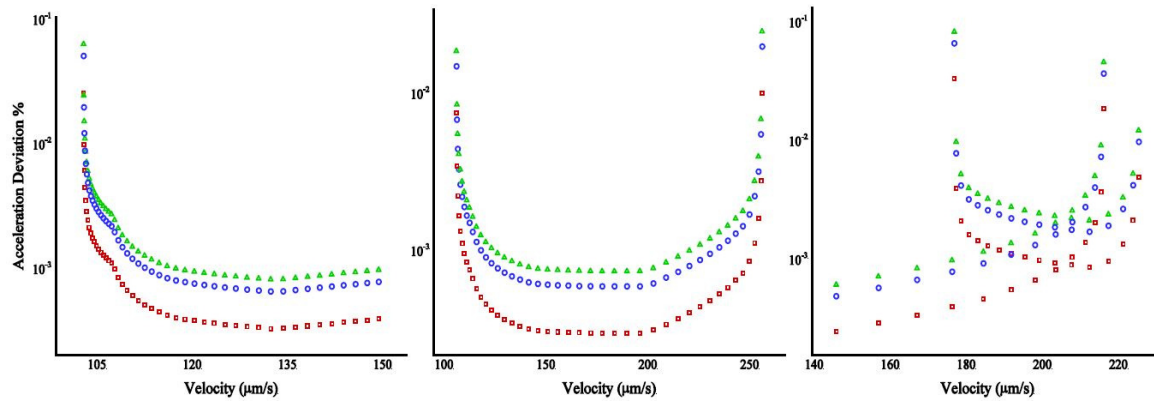
Figure 5: Percentage of Deviation of the Acceleration of the Sperm Swimming in a Nanofluid versus Base Velocity Values. Red Symbols: ϕ=0.1, T=36°C, Green Symbols: ϕ=0.2, T=36°C, Blue Symbols: ϕ=0.2, T=38°C.

5.0 CONCLUSIONS

We have derived a differential equation system for the time evolution of the experimental parallel velocity values of a sperm moving in pure water. The choice of parallel component is arbitrary and the whole framework can be extended for normal velocity or angular moments as well. This system mimics the real pattern acceptably. Furthermore, the system can also follow more sampled points via a least-squares analysis. Therefore, we can use this concept as a low-dimensional assessment of comparable experiments. On the other hand, one can investigate the obtained differential system near its equilibrium points to enjoy linearity benefits. We have sketched a trace-determinant diagram to show how we can control the dynamics by adjusting few constants in the second equation of the system. Finally, we have forced the system by an additive viscous force term due to the presence of nanoparticles in the base ow while the modified viscosity of this nanofluid suspension is modeled as a function of the viscosity of the pure water and the nanoparticles volume fraction in a single-phase analysis. It can be seen that the deviation of acceleration occurs mainly in some unique velocity values where extra volume fractions contributes to more triggered values. On the other hand this amplification is moderated by increasing the temperature of the media. One may consider the effect of solid walls and other governing phenomena by adding more forcing functions as well. The model can also be used for extrapolation of the values in short ranges. However, investigation of more complex systems needs some couplings of low-dimension models, the proposed framework can be a basis for more effective fertilization approaches.

REFERENCES

[1]   B.M. Friedrich, I.H. Riedel-Kruse, J. Howard, F. Julicher, High-precision tracking of sperm swimming fine structure provides strong test of resistive force theory, The Journal of Experimental Biology 213 (2010) 1226-1234.

[2]   P. Perona, A. Porporato, L. Ridolfi, On the Trajectory Method for the Reconstruction of Differential Equations from Time Series, Nonlinear Dynamics 23 (2000) 13-33.

[3]   A. Porporato, L. Ridolfi, Some dynamical properties of a differential model for the bursting cycle in the near-wall turbulence, Physics of Fluids 14 (2002) 4278-4283.

[4]   S. Sharafatmandjoor, N.A. Che Sidik, F. Sabetghadam, A Least-Squares-Based Immersed Boundary Approach for Complex Boundaries in the Lattice Boltzmann Method, Numerical Heat Transfer, Part B: Fundamentals 64 (2013) 407-419.

[5]   J.P. Crutchfield, B.S. McNamara, Equations of motion from a data series, Complex Systems 1 (1986) 417-452.

[6]   U. Parlitz, L. Junge, L. Kocarev, Synchronization-based parameter estimation from time series, Physical Review E 54 (1996).

[7]   J.C. Kirkman-Brown, D.J. Smith, Sperm motility: is viscosity fundamental to progress?, Molecular Human Reproduction 17 (2011) 539-544.

[8]   M.R. Abdulwahab, A Numerical Investigation of Turbulent Magnetic Nanouid Flow inside Square Straight Channel, Journal of Advanced Research in Fluid Mechanics and Thermal Sciences 1 (2014) 44-52.

[9]   N.H.M. Noh, A. Fazeli, N.A. Che Sidik, Numerical Simulation of Nanofluids for Cooling Efficiency in Microchannel Heat Sink, Journal of Advanced Research in Fluid Mechanics and Thermal Sciences 4 (2014) 13-23.

[10]   W. Penga, B. Minlia, L. Jizua, Z. Lianga, C. Wenzhenga, L. Guojiea, Comparison of Multidimensional Simulation Models for Nanofluids Flow Characteristics, Numer. Heat Trans., Part B: Fundamental (2014) 62-83.

[11]   F. Selimefendigil, H.F. Oztop, Estimation of the Mixed Convection Heat Transfer of a Rotating Cylinder in a Vented Cavity Subjected to Nanofluid by Using Generalized Neural Networks. Numerical Heat Transfer, Part A: Applications (2014) 165-185.

[12]   F. Alfieri, S. Gianini, M.K. Tiwari, T. Brunschwiler, B. Michel, D. Poulikakos, Computational Modeling of Hot-Spot Identification and Control in 3-D Stacked Chips with Integrated Cooling, Numerical Heat Transfer, Part A: Applications (2014) 201-215.

[13]   S. Sivasankarana, K.L. Pana, Natural Convection of Nanofluids in a Cavity with Non-uniform Temperature Distributions on Side Walls, Numerical Heat Transfer, Part A: Applications (2014) 247-268.

[14]   A. Kazemi-Beydokhtia, H.A. Namaghia, S.Z. Herisa, Identification of the Key Variables on Thermal Conductivity of CuO Nanofluid by a Fractional Factorial Design Approach. Numer. Numerical Heat Transfer, Part B: Fundamentals (2014) 480-495.

[15]   H.C. Brinkman, The viscosity of concentrated suspensions and solutions. The Journal of Chemical Physics 20 (1952) 571-581.

[16]   N. Bachok, A. Ishak, I. Pop, Stagnation-point ow over a stretching/shrinking sheet in a nanouid, Nanoscale Research Letters 6 (2011) 623.

[17] M. Mehrabi, M. Sharifpur, J.P. Meyer, Viscosity of nanofluids based on an artificial intelligence model, International Communications in Heat and Mass Transfer 43 (2013) 16-21.

[18] N.A. Che Sidik, M. Khakbaz, L. Jahanshaloo, S. Samion, N.A. Darus, Simulation of forced convection in a channel with nanofluid by the lattice Boltzmann method, Nanoscale Research Letters 8 (2013) 178.

[19] H.G.R. Kefayati, Simulation of Ferrofluid Heat Dissipation Effect on Natural Convection at an Inclined Cavity Filled with Kerosene/Cobalt Utilizing the Lattice Boltzmann Method, Numerical Heat Transfer, Part A: Applications (2014) 509-530.

[20] W. Penga, L. Jizua, B. Minlia, W. Yuyanab, H. Chengzhia, Z. Lianga, Numerical Simulation on the Flow and Heat Transfer Process of Nanofluids Inside a Piston Cooling Gallery, Numerical Heat Transfer, Part A: Applications (2014) 378-400.

[21] T. Eisenhammer, A. Hubler, N. Packard, K.A.S. Kelso, Modeling Experimental Time Series with Ordinary Differential Equations. Biological Cybernetics 65 (1991) 107-112.

[22] M.W. Hirsch, S. Smale, R.L. Devaney, Differential Equations, Dynamical Systems, and an Introduction to Chaos, Third Edition, Elsevier Academic Press, 2012.

[23] J. Gray, G.J. Hancock, The propulsion of sea-urchin spermatozoa. Journal of Experimental Biology 32 (1955) 802-814.

[24] E. Lauga, W.R. DiLuzio, G.M. Whitesides, H.A. Stone, Swimming in Circles: Motion of Bacteria near Solid Boundaries, Biophysical Journal 90 (2006) 400-412.

[25] J. Lee, K.S. Hwang, S.P. Jang, B.H. Lee, J.H. Kim, S.U.S. Choi, C.J. Choi, Effective viscosities and thermal conductivities of aqueous nanofluids containing low volume concentrations of Al_2O_3 nanoparticles, International Journal of Heat and Mass Transfer 51 (2008) 2651-2656.